Electronic Supplementary Material (ESI) for New Journal of Chemistry.

Supporting Information For:

A sulfonic acid functionalized zirconium-based metal organic framework for the selective detection of copper(II) ion

*Abhijeet Rana,[a] Soutick Nandi[ab] and Shyam Biswas[a]**

[a] Department of Chemistry, Indian Institute of Technology Guwahati, Guwahati, 781039 Assam, India.

[b] *Department of Applied Science, Ghani Khan Choudhury Institute of Engineering & Technology, Malda, 732141 West Bengal, India.*

* Corresponding author. Tel: +91-3612583309, Fax: +91-3612582349.

E-mail address: sbiswas@iitg.ac.in

Materials and General Methods:

All the reagents and solvents were purchased from commercial sources and used without purification, except the $H_2BPDC\text{-}(SO_3H)_2$ ligand which was synthesized by following a reported literature.[1] The Attenuated Total Reflectance Infrared (ATR-IR) spectra were recorded using PerkinElmer UATR Two at ambient condition in the region 400-4000 cm^{-1}. The notations used for characterization of the bands are broad (br), strong (s), very strong (vs), medium (m), weak (w) and shoulder (sh). FE-SEM images were captured with a Zeiss (Zemini) scanning electron microscope. Thermogravimetric analysis (TGA) was carried out with an SDT Q600 V20.9 Build 20 thermogravimetric analyzer in the temperature range of 25-700 °C in an argon atmosphere at the rate of 10 °C min^{-1}. Rigaku Smartlab X-ray diffractometer (model TTRAX III) was employed for powder X-ray diffraction (PXRD) measurements at 50 kV, 100 mA using Cu-*K*α (λ = 1.5406 Å) radiation. N_2 sorption isotherms were recorded by using Quantachrome Autosorb iQ-MP volumetric gas adsorption equipment at −196 °C. Before the sorption analysis, the degassing of the compound was carried out at 100°C under high vacuum for 12 h. Fluorescence sensing studies were performed with a HORIBA JOBIN YVON Fluoromax-4 spectrofluorometer. A Bruker Avance III 600 NMR spectrometer was used for recording ^1H NMR spectra at 600 MHz. Pawley refinement was carried out using Materials Studio software.

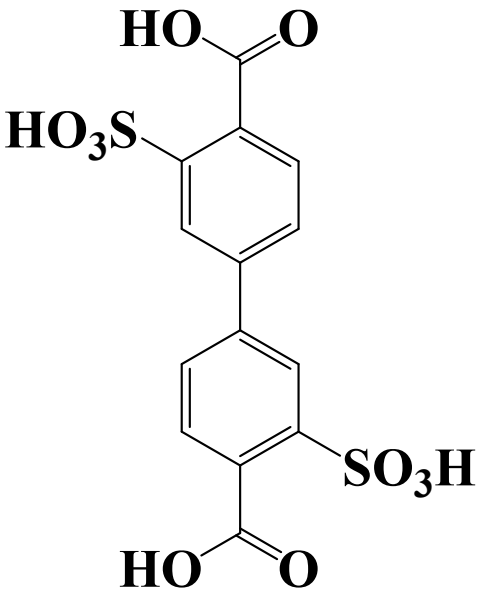

Figure S1. Structure of linker ($H_2BPDC\text{-}(SO_3H)_2$).

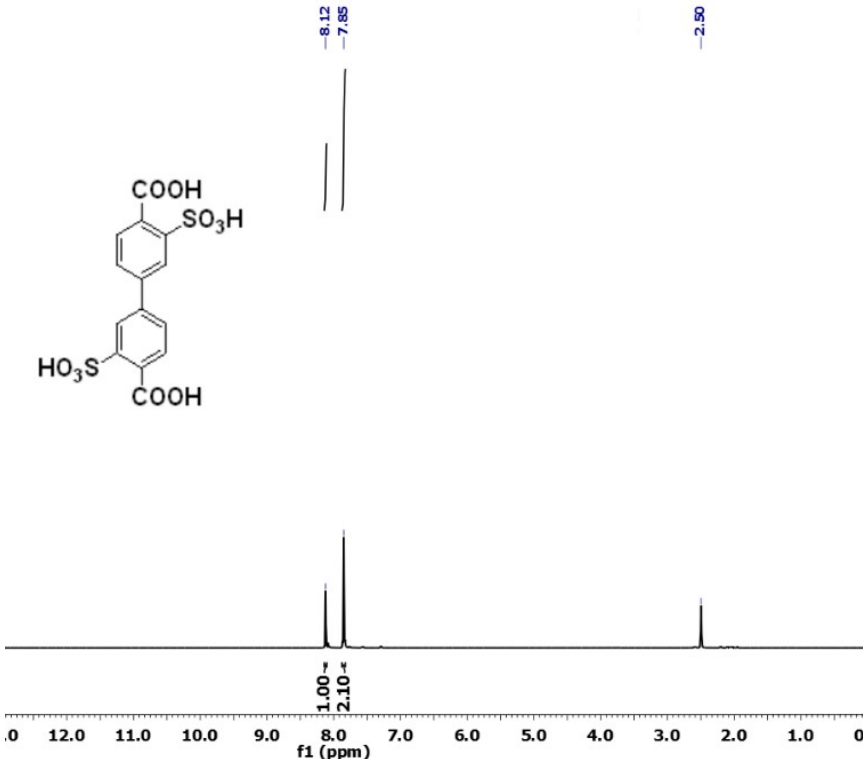

Figure S2. ^{1}H NMR of linker ($H_2BPDC\text{-}(SO_3H)_2$).

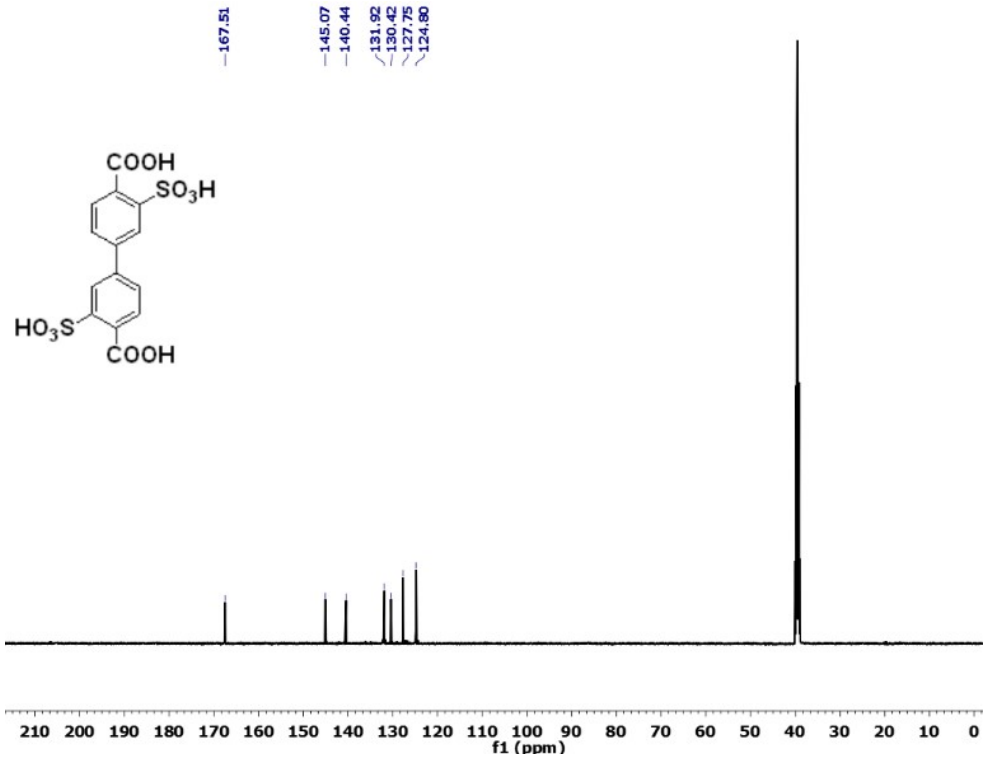

Figure S3. ^{13}C NMR of linker ($H_2BPDC\text{-}(SO_3H)_2$).

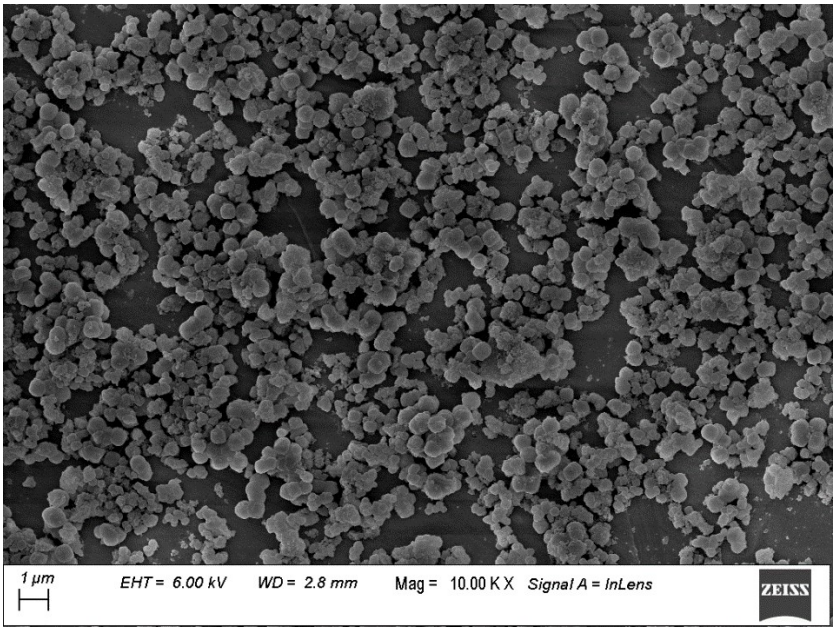

Figure S4. FESEM image of **1′**.

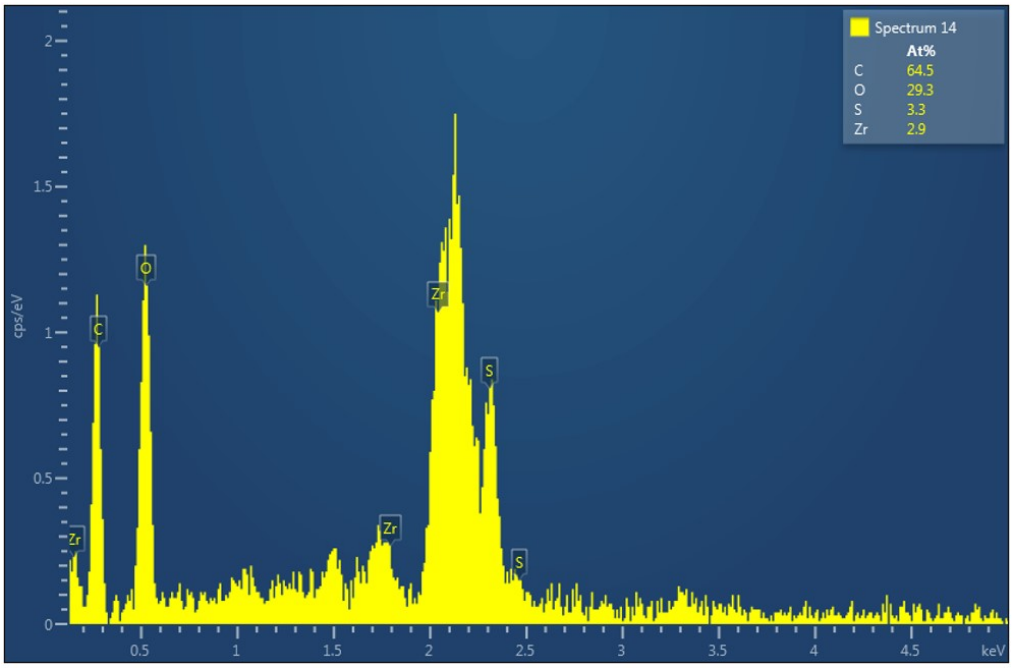

Figure S5. EDX spectrum of **1′**.

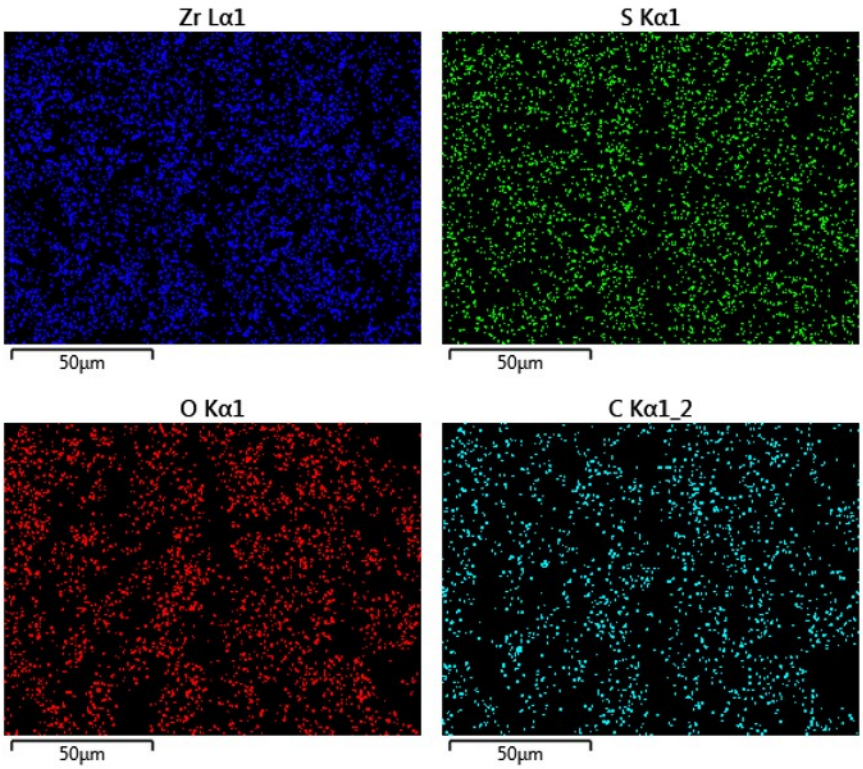

Figure S6. EDX elemental mapping of **1′**.

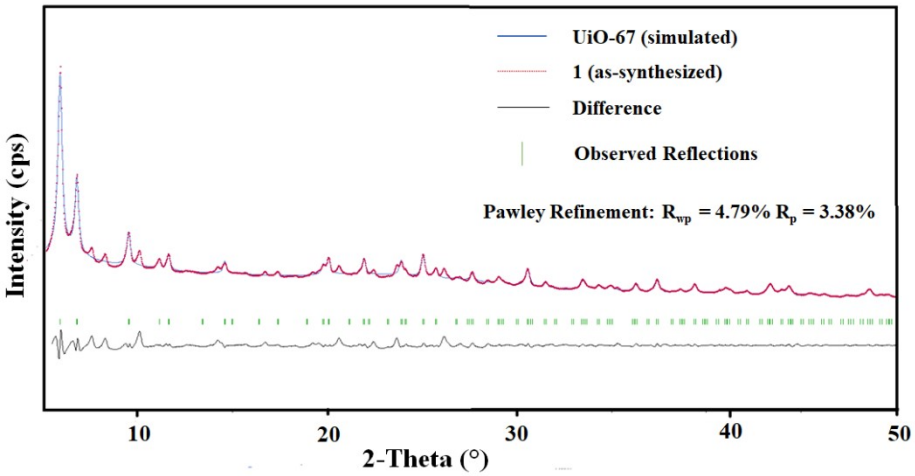

Figure S7. Pawley fit for the PXRD pattern of as-synthesized **1**. Blue lines and red dots denote simulated and observed patterns, respectively. The peak positions and difference plot are displayed at middle (R_p = 3.38 %, R_{wp} = 4.79 %).

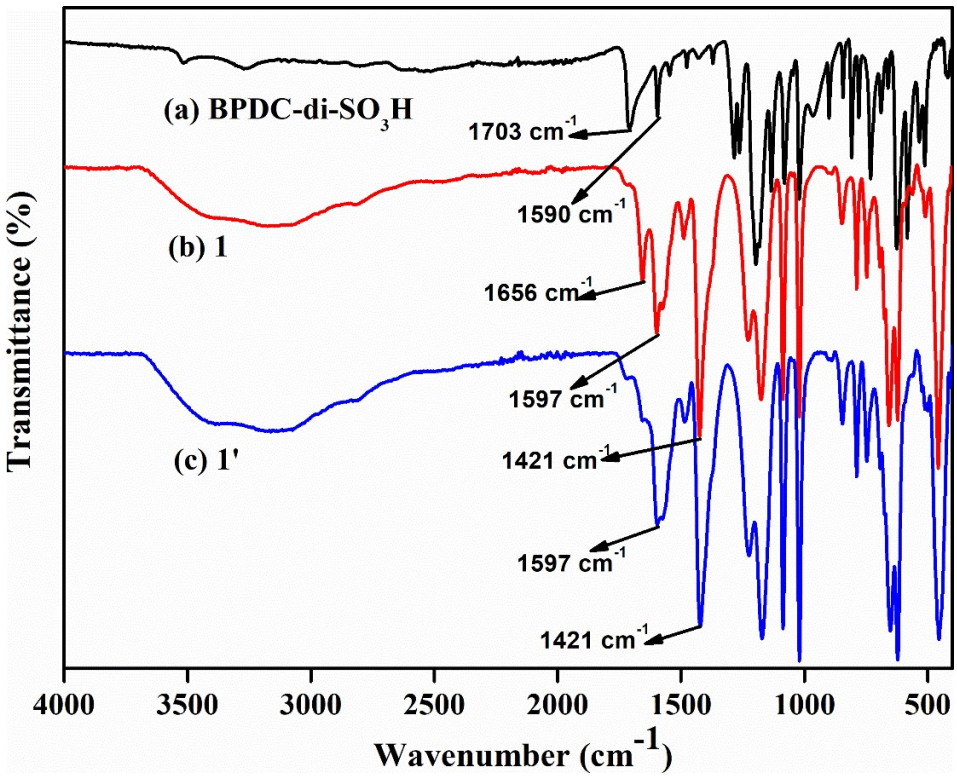

Figure S8. FT-IR spectra of (a) $H_2BPDC\text{-}(SO_3H)_2$ ligand (black), (b) as-synthesized **1** (red) and (c) activated **1′** (blue).

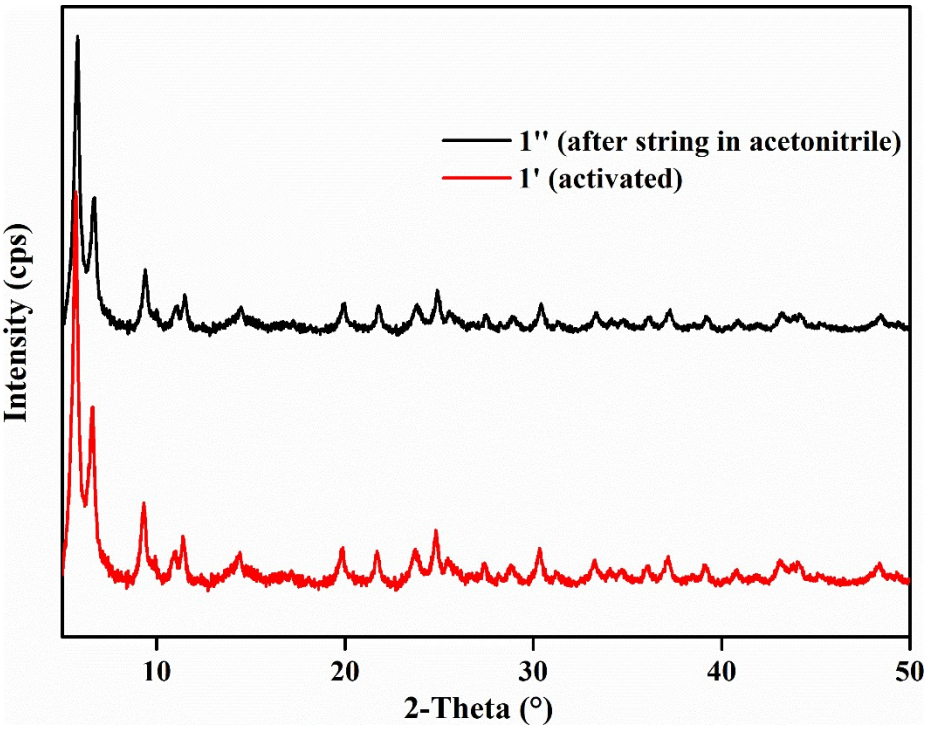

Figure S9. PXRD pattern of **1′** (red) and **1′′** (black).

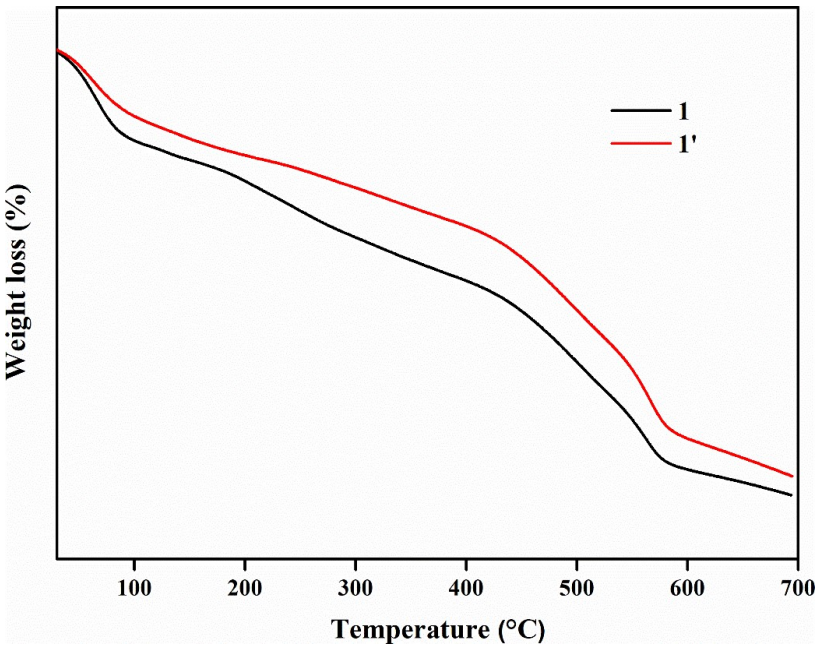

Figure S10. TGA curves of as-synthesized **1** (red) and activated **1′** (black) recorded in a nitrogen atmosphere in the temperature range of 30-700 °C at a heating rate of 10 °C min^{-1}.

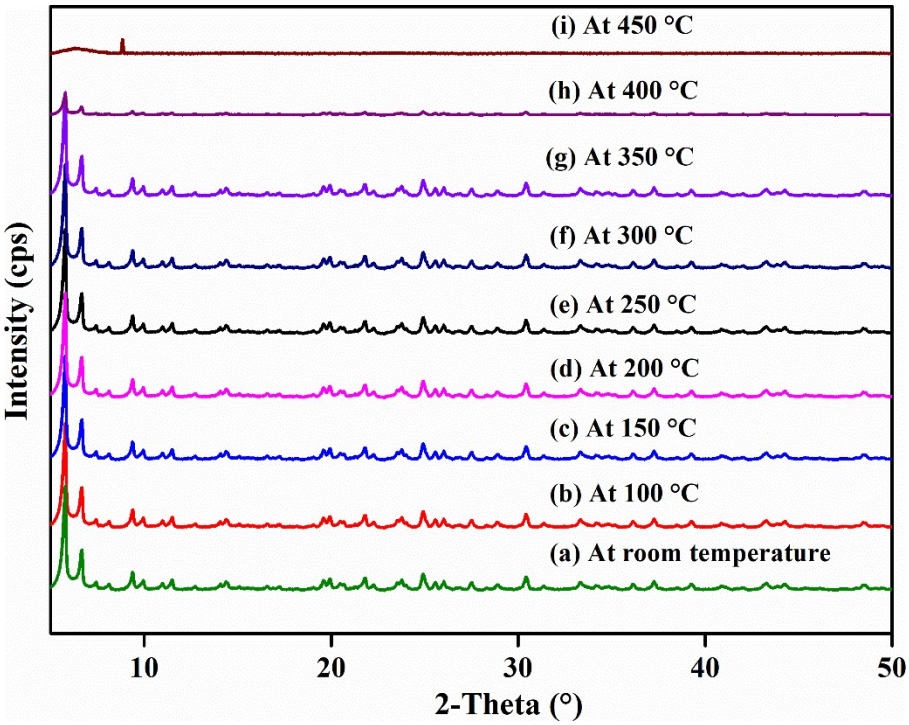

Figure S11. Temperature dependent PXRD patterns of **1′** up to 450 °C.

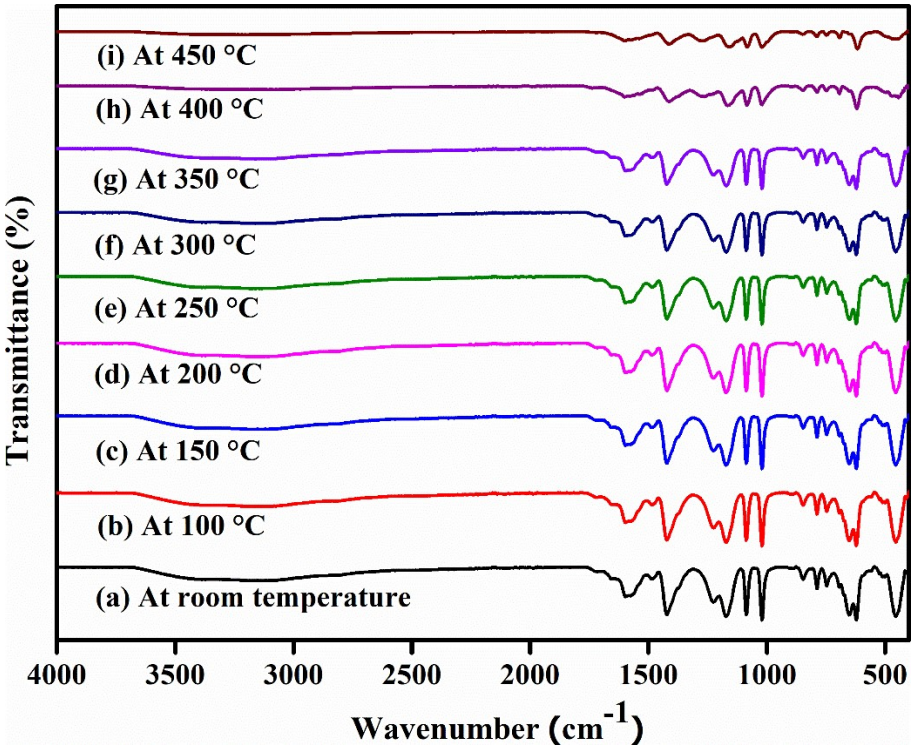

Figure S12. Temperature dependent FT-IR spectra of **1′** up to 450 °C.

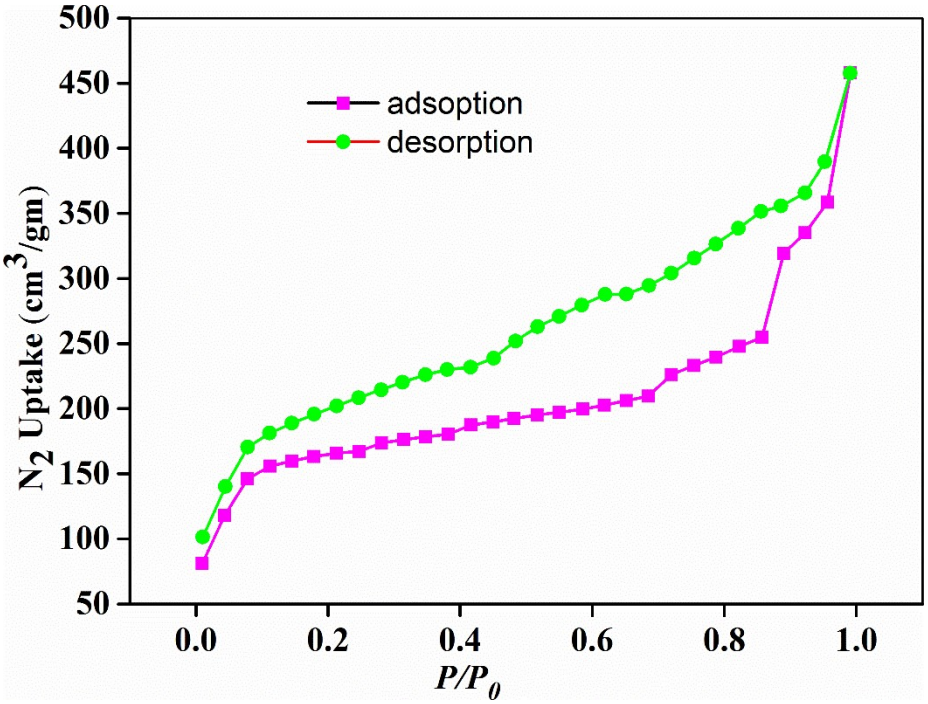

Figure S13. N_2 adsorption (green circles) and desorption (pink circles) isotherms of thermally activated **1′** recorded at –196 °C.

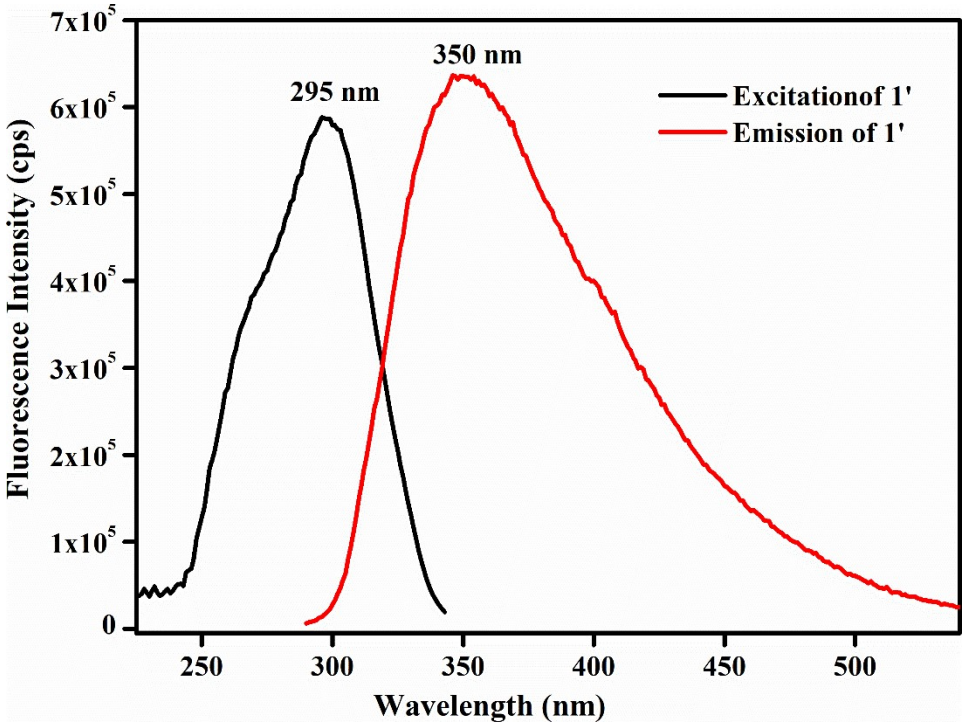

Figure S14. Fluorescence excitation (black) and emission (red) spectra of **1′**.

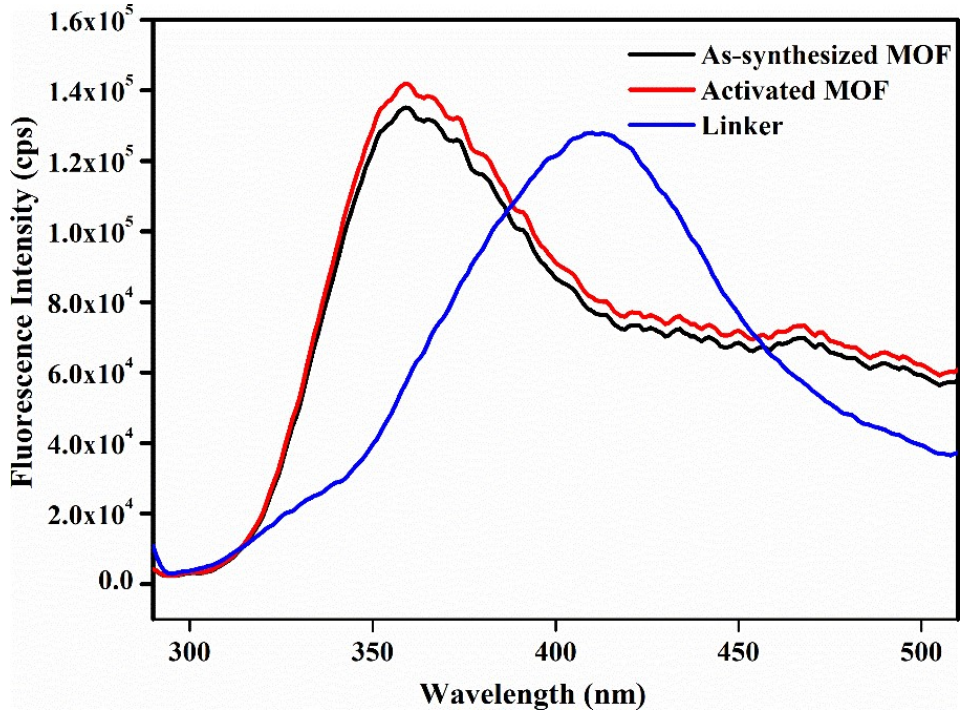

Figure S15. Solid state fluorescence spectra of **1** (black), **1′** (red) and linker (blue).

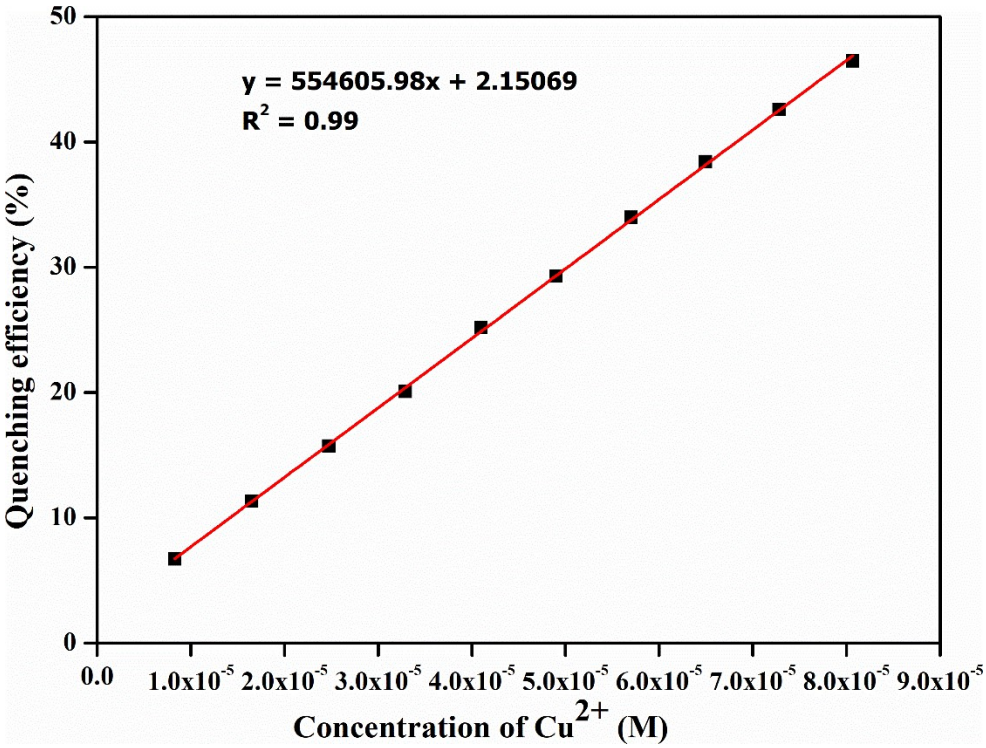

Figure S16. Stern-Volmer plot for the fluorescence emission quenching of **1′** in presence of Cu^{2+} solution.

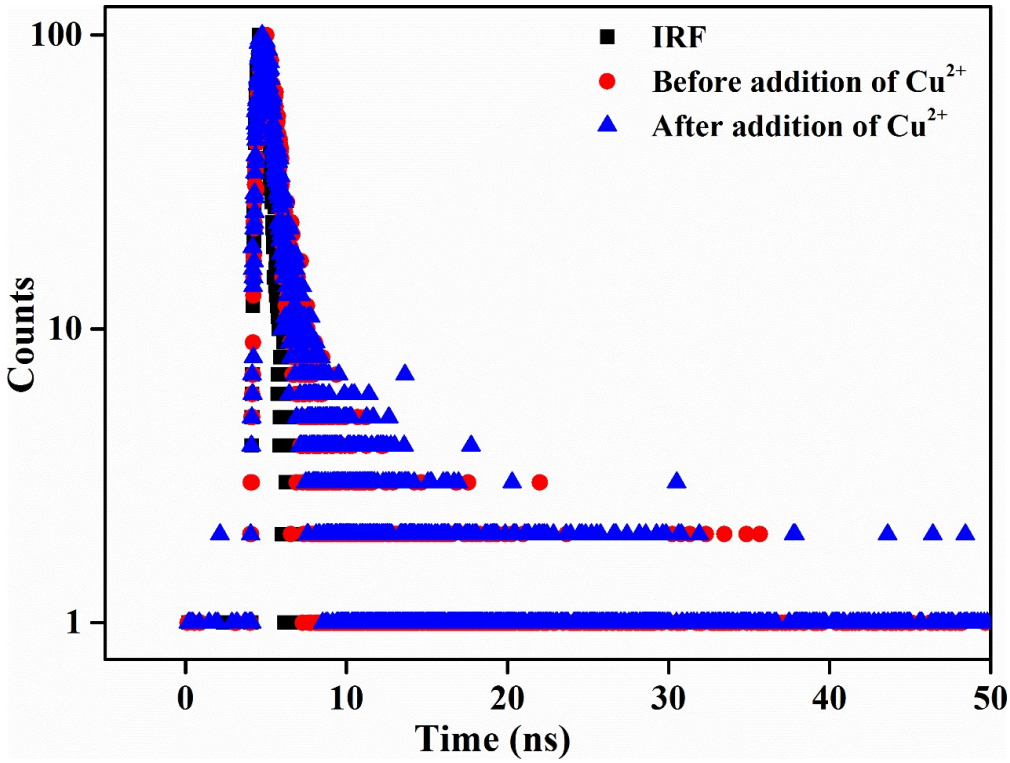

Figure S17. Lifetime decay profile of **1′** before and after the addition of 2 mM Cu^{2+} acetonitrile solution.

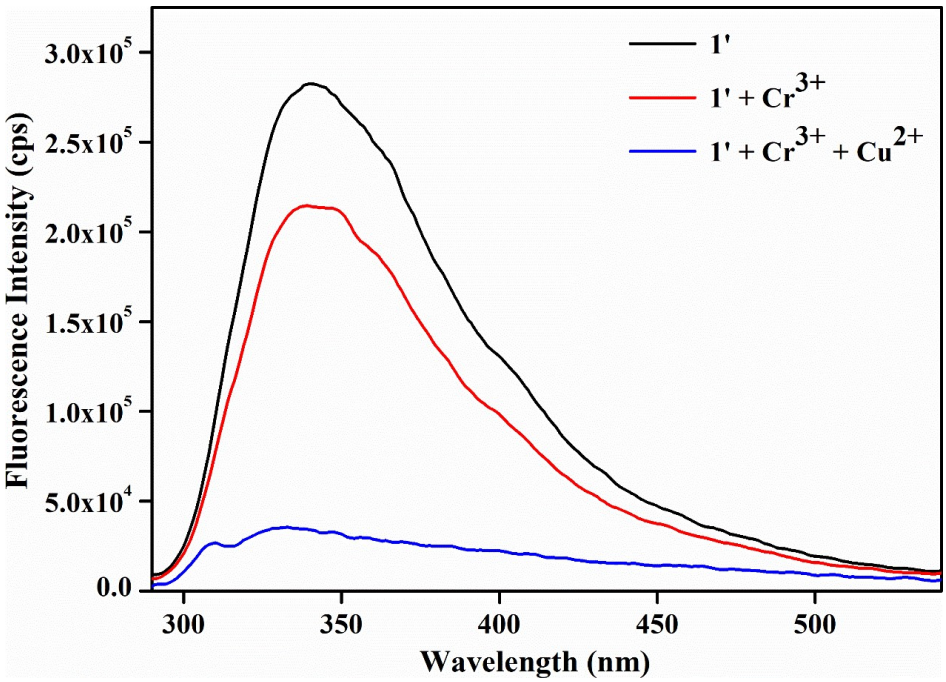

Figure S18. Fluorescence intensity of **1′** dispersed in acetonitrile after addition of 2 mM solution of $Cu(NO_3)_2$ in acetonitrile (500 µL) in presence of 2 mM solution of $Cr(NO_3)_3$ in acetonitrile (500 µL).

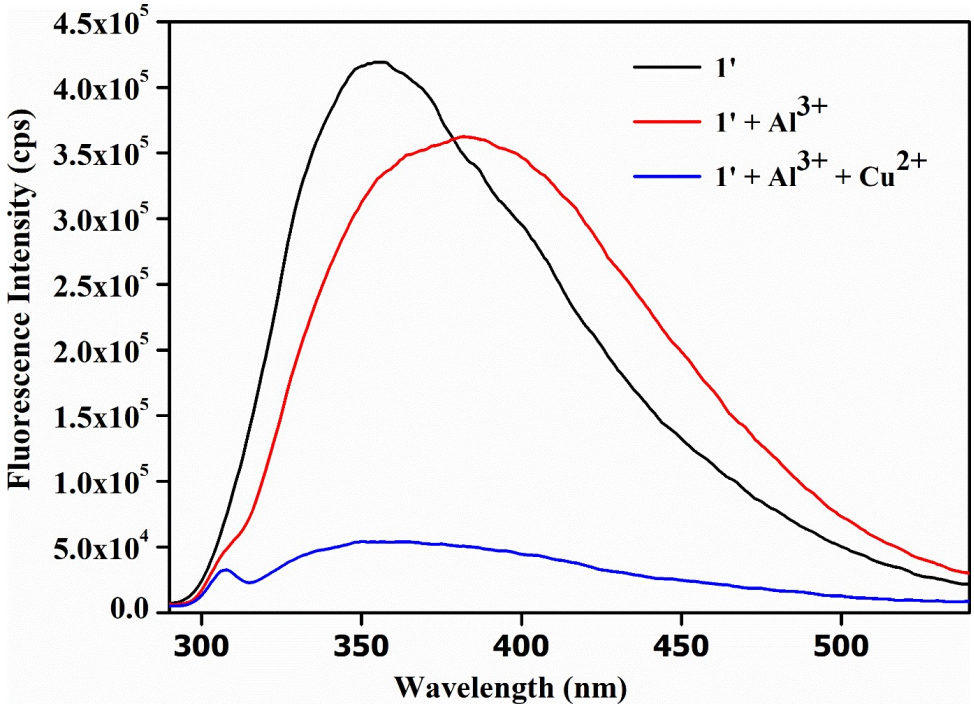

Figure S19. Fluorescence intensity of **1′** dispersed in acetonitrile after addition of 2 mM solution of $Cu(NO_3)_2$ in acetonitrile (500 µL) in presence of 2 mM solution of $Al(NO_3)_3$ in acetonitrile (500 µL).

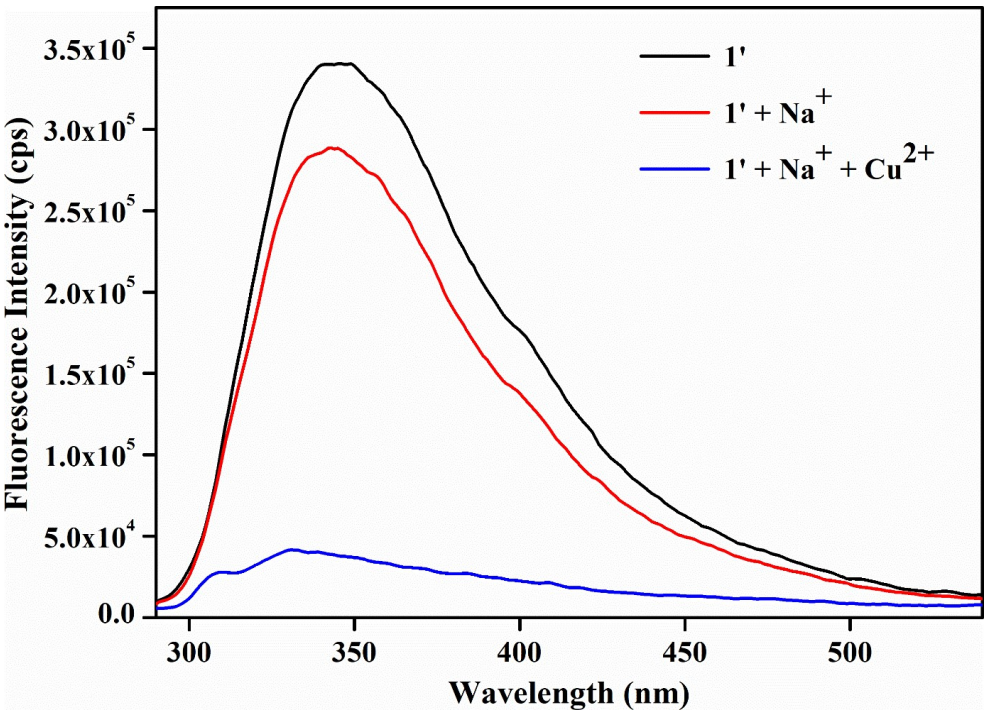

Figure S20. Fluorescence intensity of **1′** dispersed in acetonitrile after addition of 2 mM solution of $Cu(NO_3)_2$ in acetonitrile (500 µL) in presence of 2 mM solution of $NaNO_3$ in acetonitrile (500 µL).

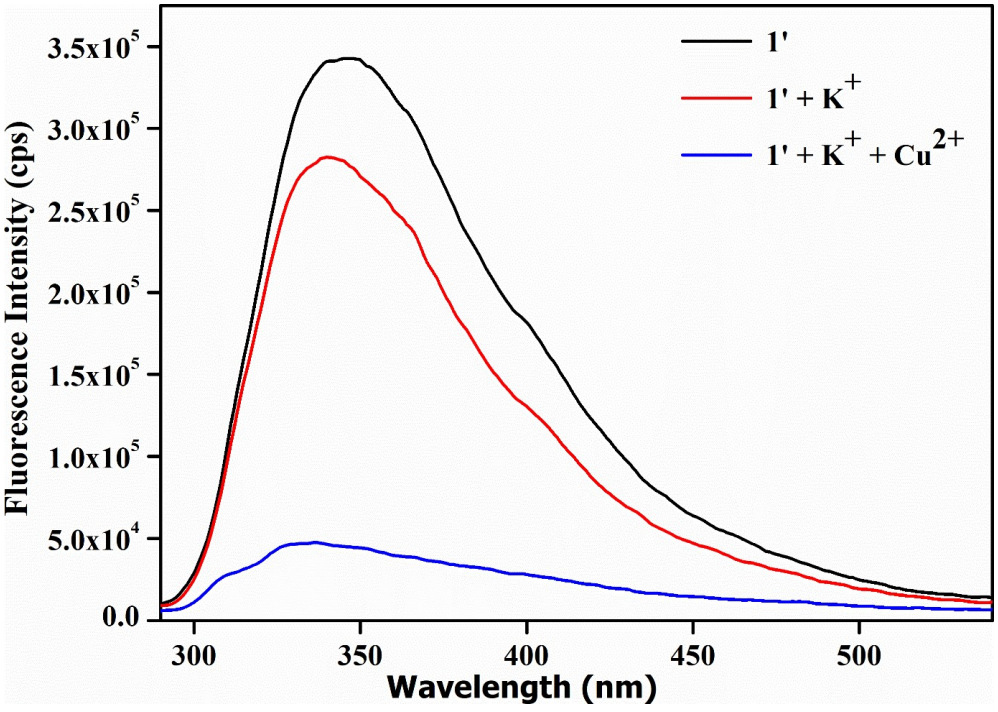

Figure S21. Fluorescence intensity of **1′** dispersed in acetonitrile after addition of 2 mM solution of $Cu(NO_3)_2$ in acetonitrile (500 µL) in presence of 2 mM solution of KNO_3 in acetonitrile (500 µL).

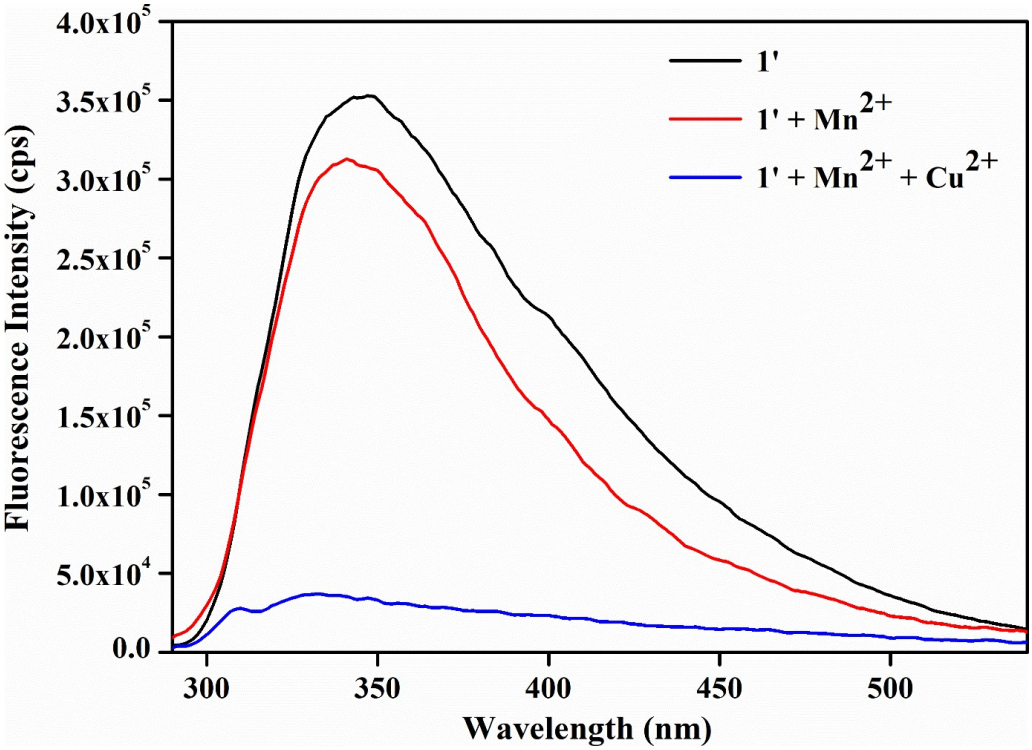

Figure S22. Fluorescence intensity of **1′** dispersed in acetonitrile after addition of 2 mM solution of $Cu(NO_3)_2$ in acetonitrile (500 µL) in presence of 2 mM solution of $Mn(NO_3)_3$ in acetonitrile (500 µL).

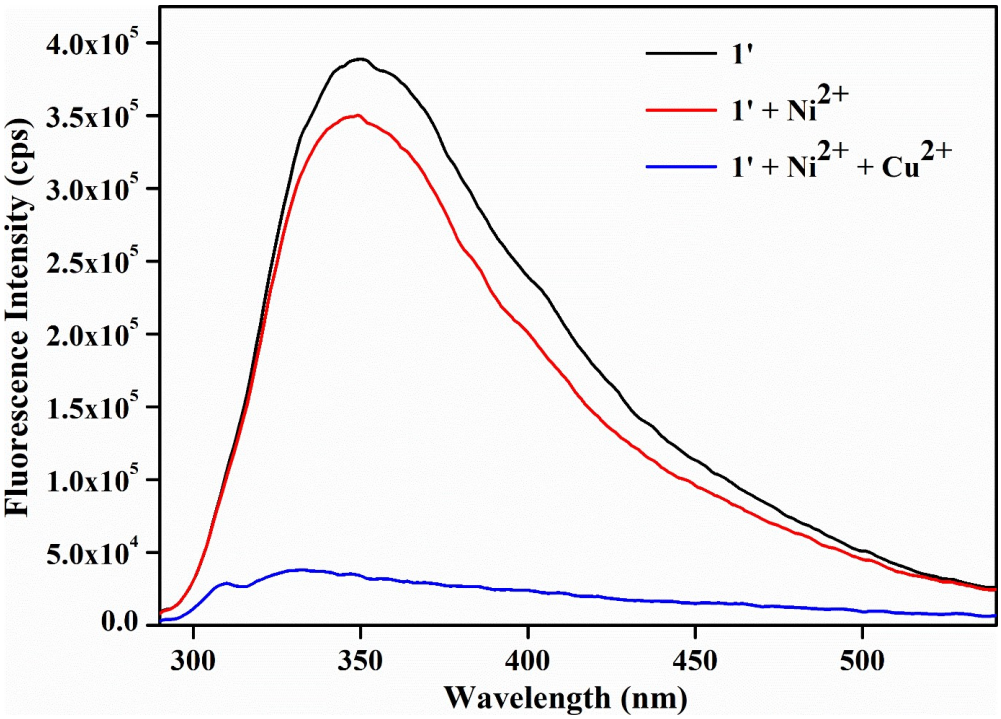

Figure S23. Fluorescence intensity of **1′** dispersed in acetonitrile after addition of 2 mM solution of $Cu(NO_3)_2$ in acetonitrile (500 µL) in presence of 2 mM solution of $Ni(NO_3)_2$ in acetonitrile (500 µL).

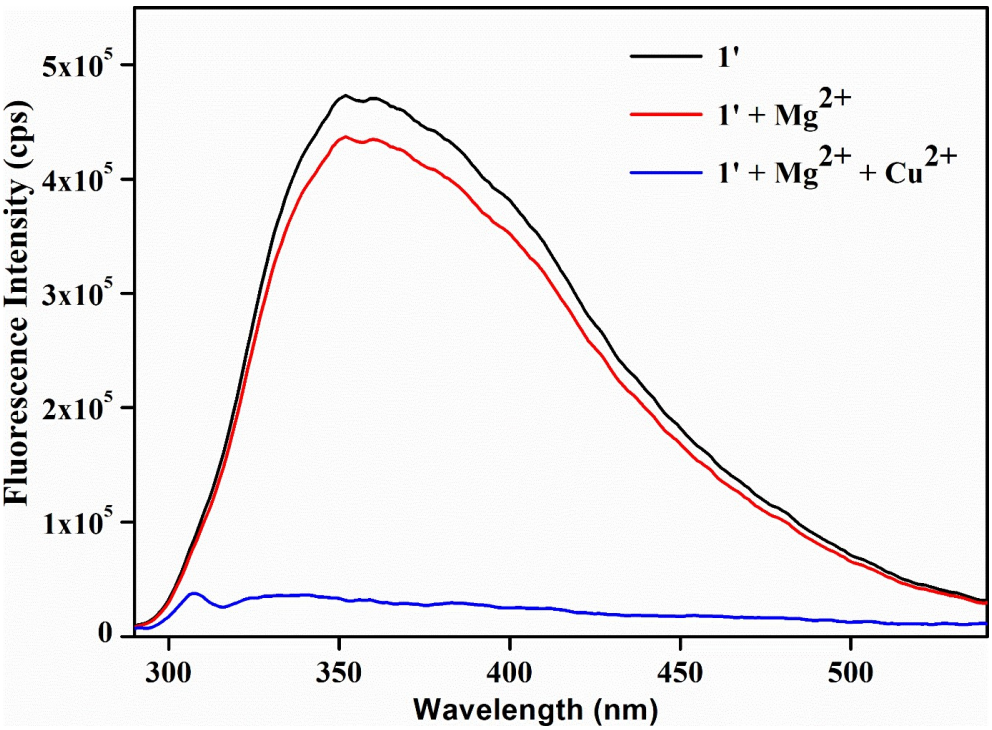

Figure S24. Fluorescence intensity of **1′** dispersed in acetonitrile after addition of 2 mM solution of $Cu(NO_3)_2$ in acetonitrile (500 µL) in presence of 2 mM solution of $Mg(NO_3)_2$ in acetonitrile (500 µL).

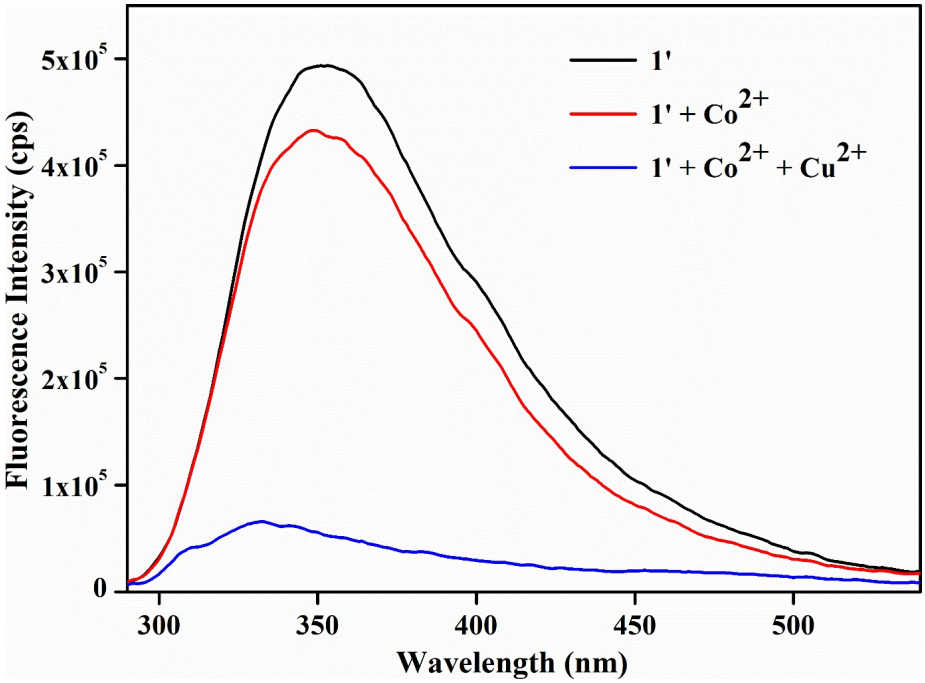

Figure S25. Fluorescence intensity of **1′** dispersed in acetonitrile after addition of 2 mM solution of $Cu(NO_3)_2$ in acetonitrile (500 µL) in presence of 2 mM solution of $Co(NO_3)_2$ in acetonitrile (500 µL).

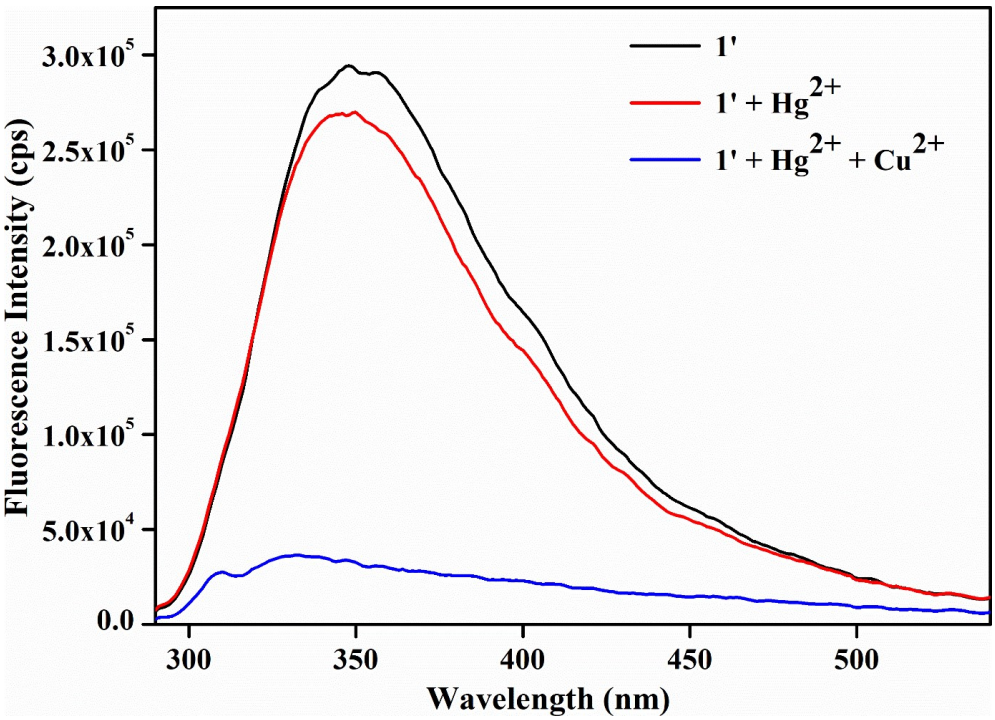

Figure S26. Fluorescence intensity of **1′** dispersed in acetonitrile after addition of 2 mM solution of $Cu(NO_3)_2$ in acetonitrile (500 µL) in presence of 2 mM solution of $Hg(NO_3)_2$ in acetonitrile (500 µL).

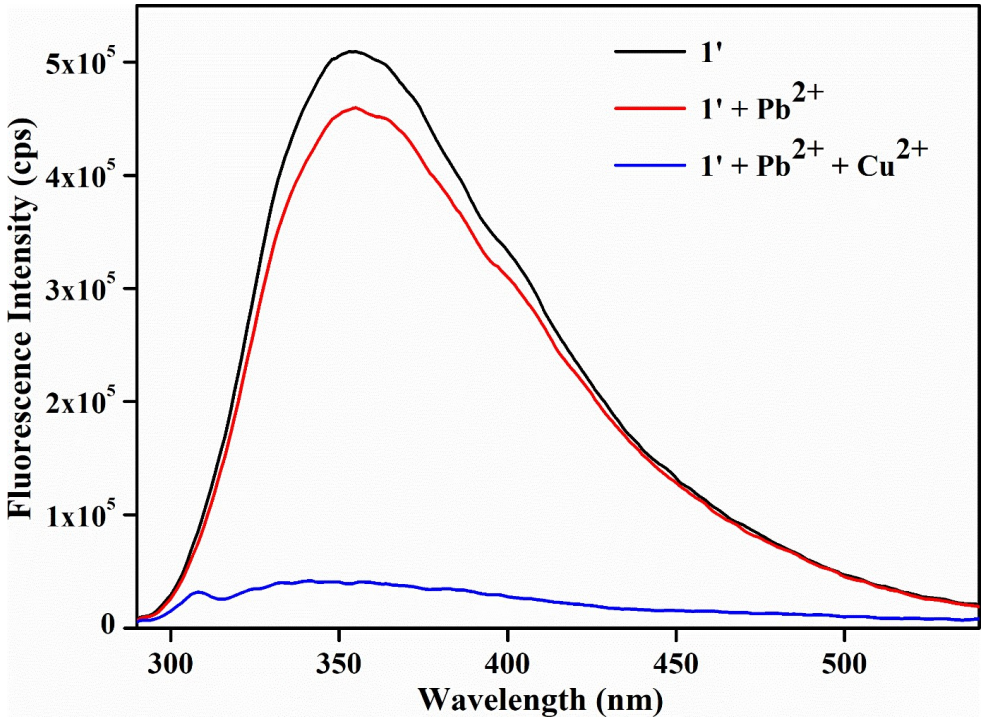

Figure S27. Fluorescence intensity of **1′** dispersed in acetonitrile after addition of 2 mM solution of $Cu(NO_3)_2$ in acetonitrile (500 µL) in presence of 2 mM solution of $Pb(NO_3)_2$ in acetonitrile (500 µL).

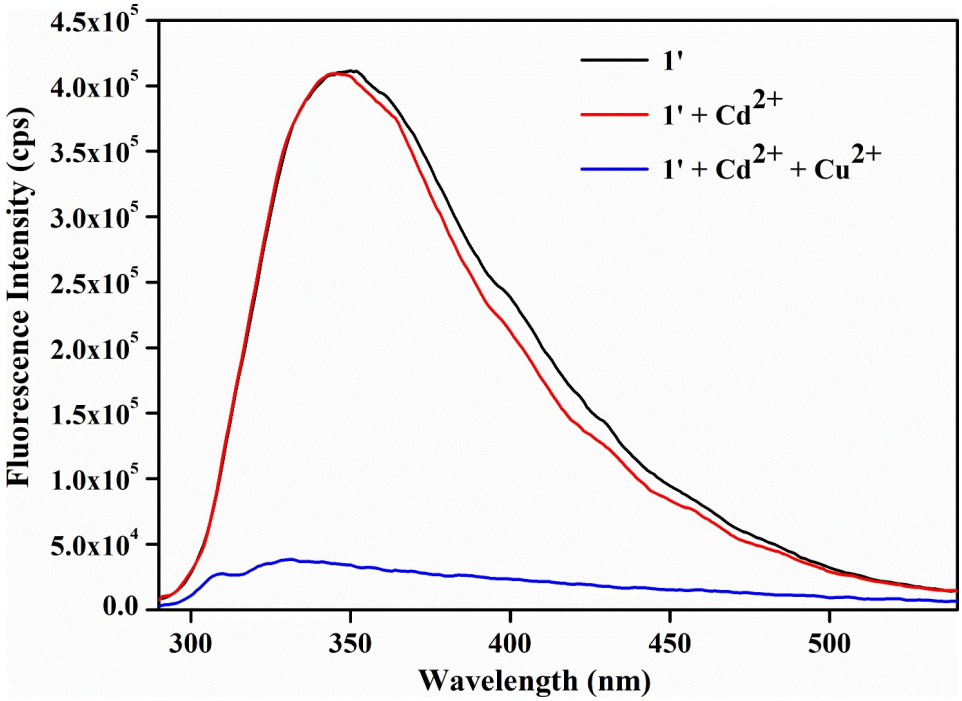

Figure S28. Fluorescence intensity of **1′** dispersed in acetonitrile after addition of 2 mM solution of $Cu(NO_3)_2$ in acetonitrile (500 µL) in presence of 2 mM solution of $Cd(NO_3)_2$ in acetonitrile (500 µL).

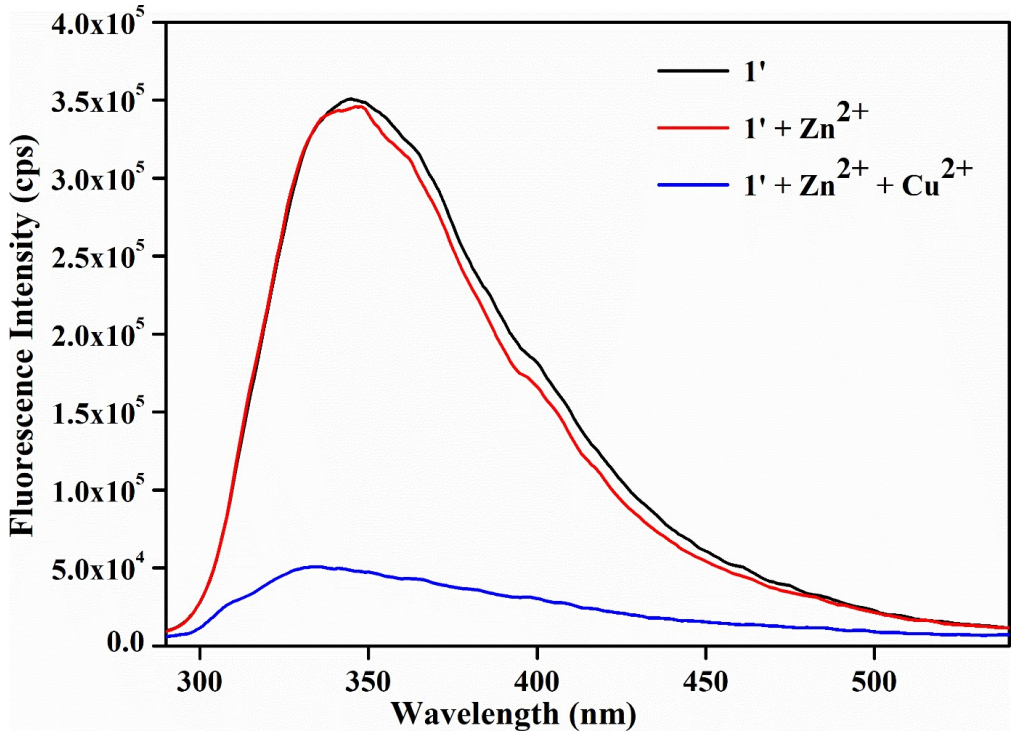

Figure S29. Fluorescence intensity of **1′** dispersed in acetonitrile after addition of 2 mM solution of $Cu(NO_3)_2$ in acetonitrile (500 µL) in presence of 2 mM solution of $Zn(NO_3)_2$ in acetonitrile (500 µL).

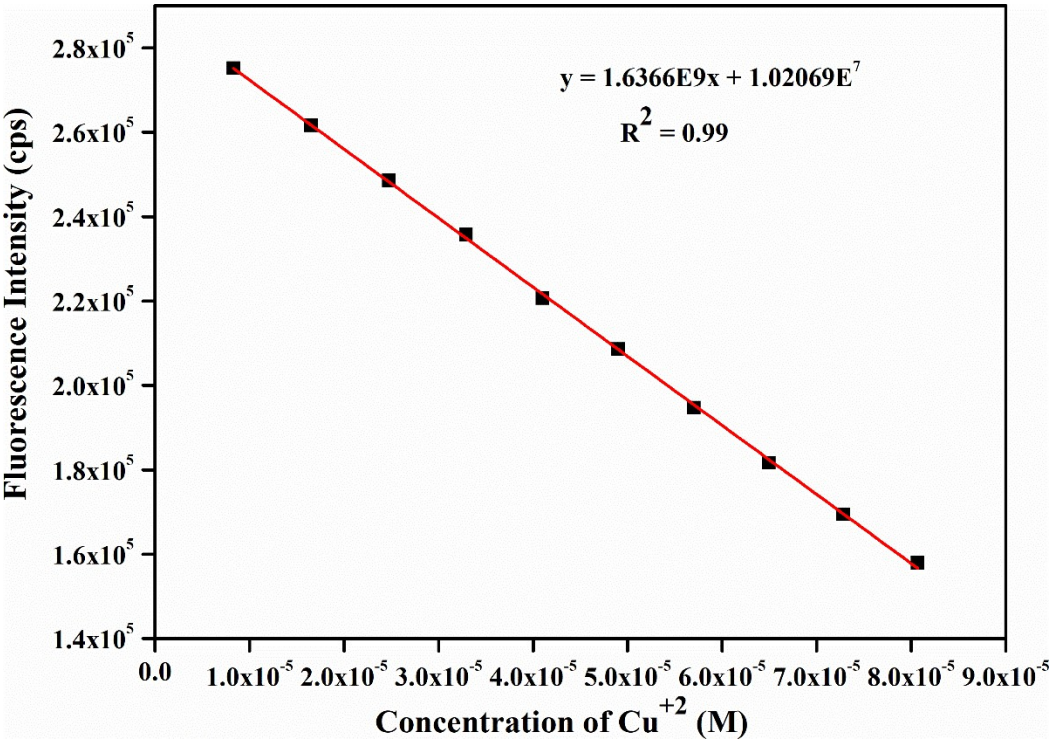

Figure S30. Change in the fluorescence intensity of **1′** as a function of Cu^{2+} concentration.

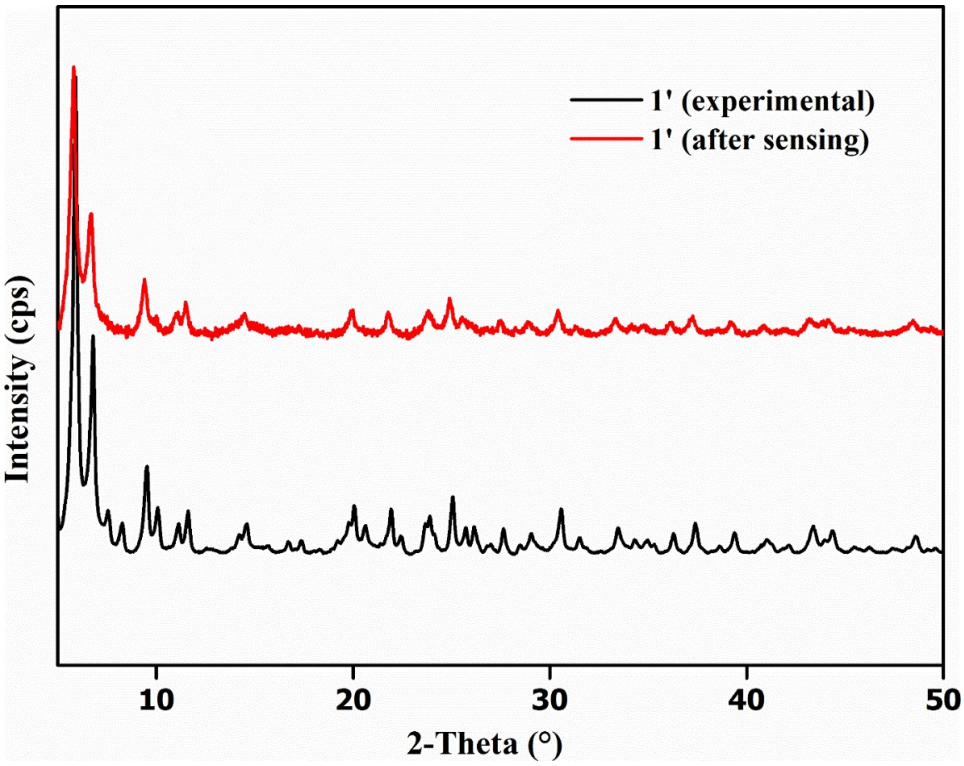

Figure S31. The PXRD pattern of **1′** (black line) and the PXRD pattern of **1′** after sensing (red line).

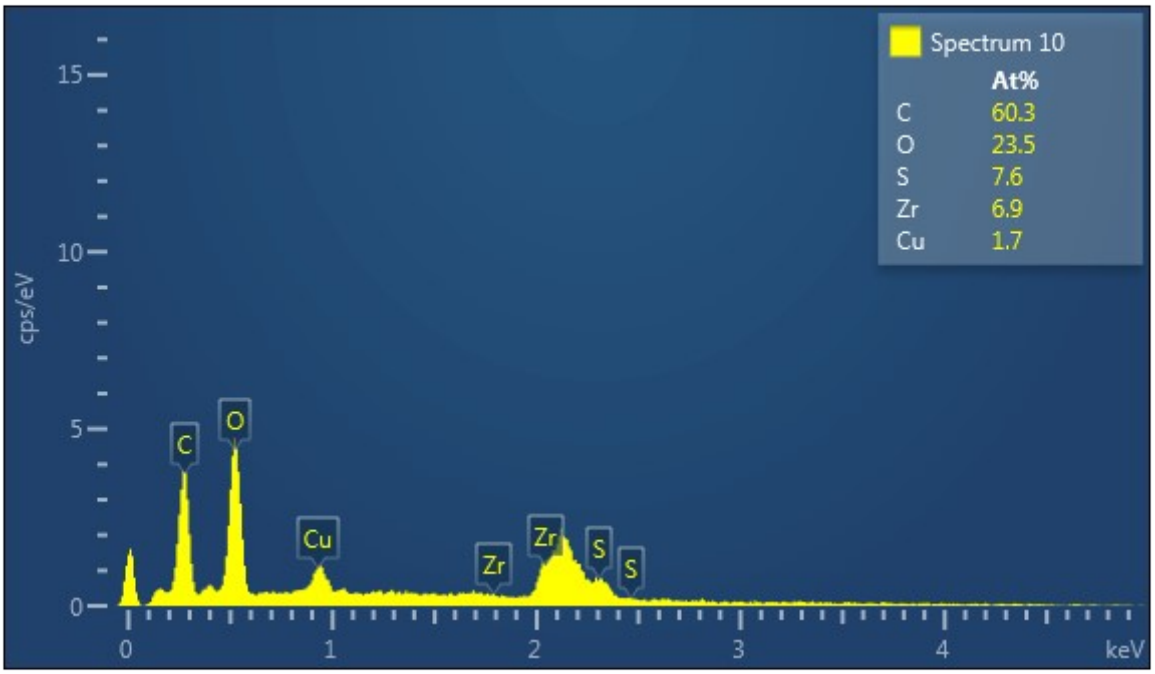

Figure S32. EDX spectrum of **1′** after treatment with Cu^{2+}.

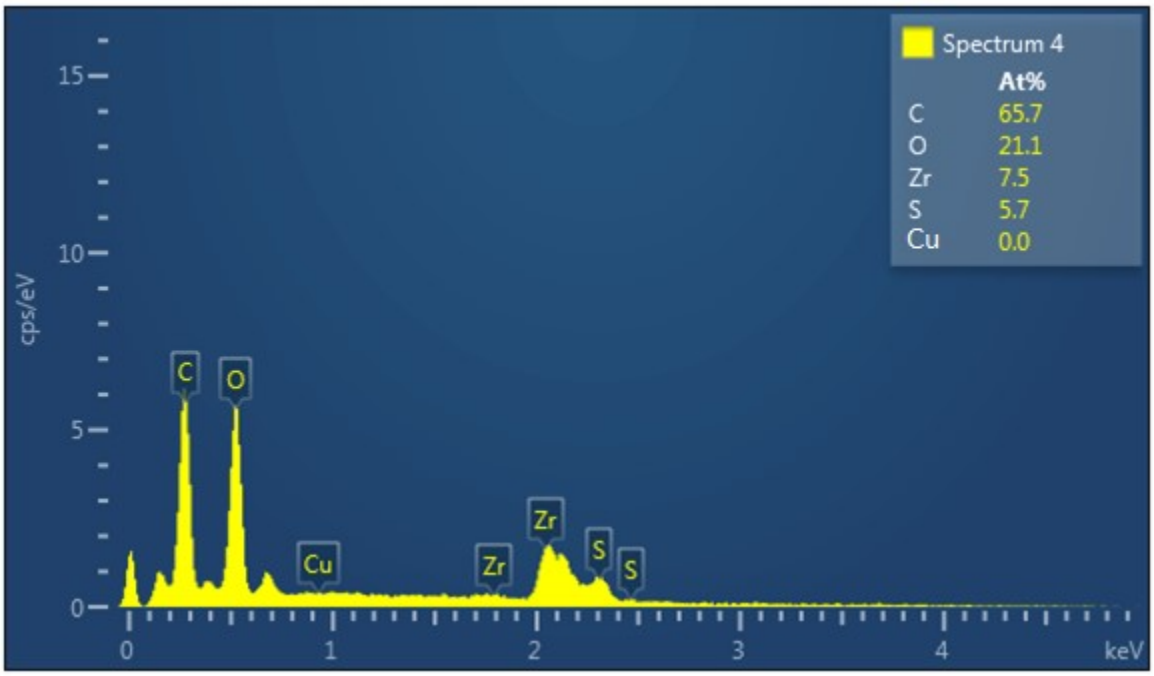

Figure S33. EDX spectrum of the recyclable sample of **1′**.

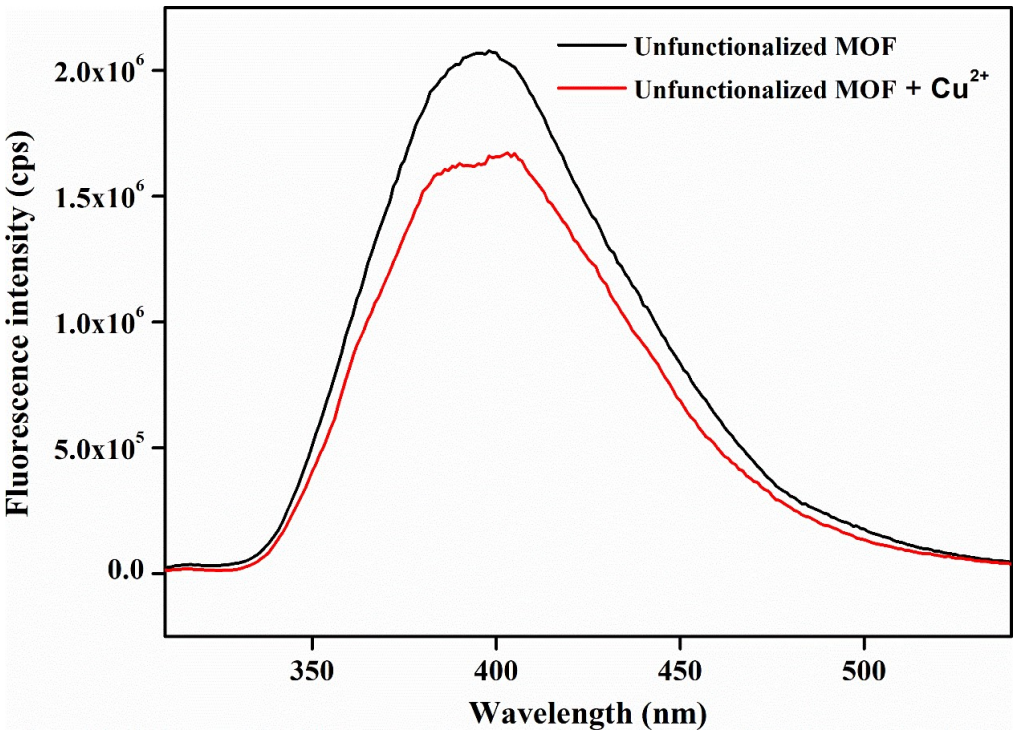

Figure S34. Fluorescence intensity of un-functionalized MOF with BPDC linker dispersed in acetonitrile and after addition of 2 mM solution of $Cu(NO_3)_2$ in acetonitrile (500 µL).

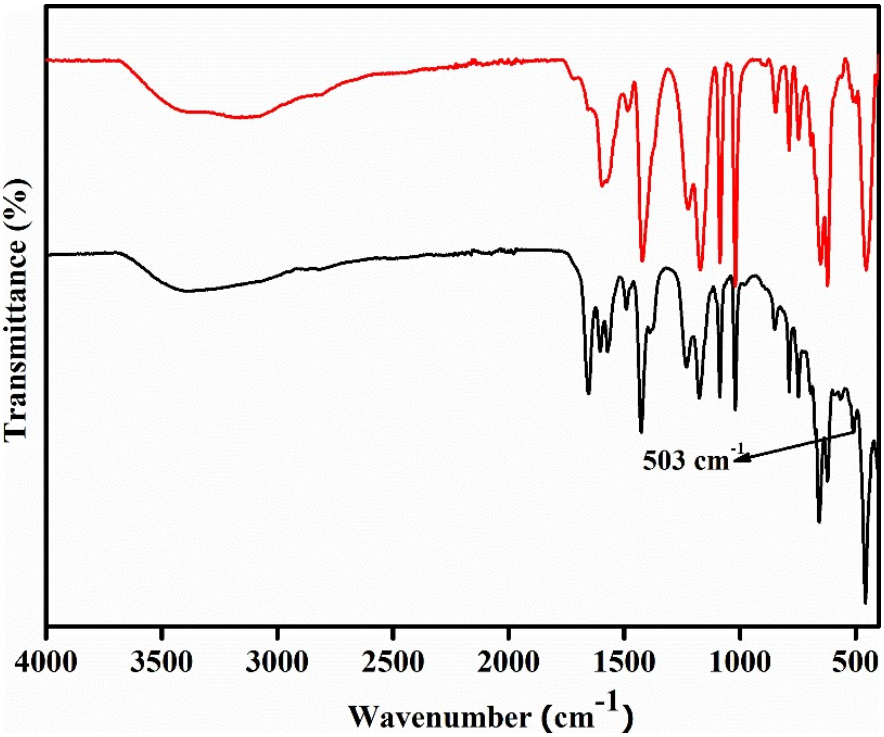

Figure S35. FT-IR spectra of MOF after treatment with Cu^{2+}.

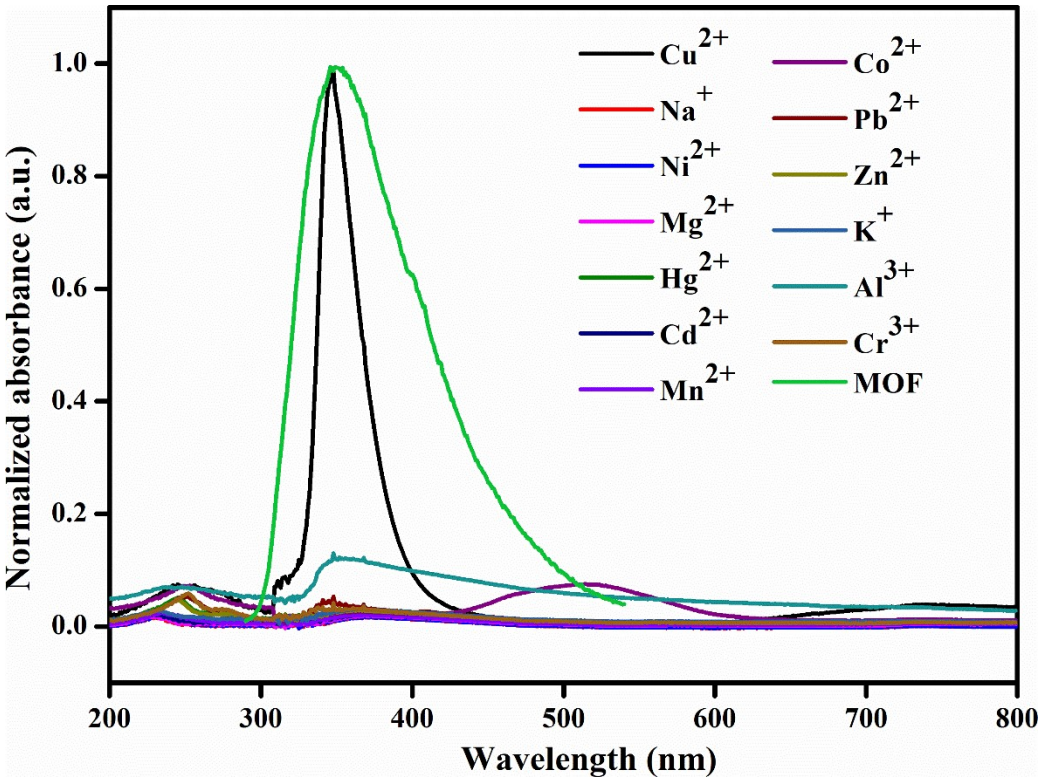

Figure S36. Fluorescence emission spectra of MOF and absorption all the analytes in acetonitrile.

Table S1. Fluorescence lifetimes of **1′** before and after the addition of Cu^{2+} solution (λ_{ex} = 270 nm, pulsed diode laser).

Volume of Cu^{2+} solution added (μL)	B_1	a_1	τ_1 (ns)	$\langle\tau\rangle^*$ (ns)	χ^2
0	88.06	1	0.82	0.82	1.097
75	0.39	1	0.45	0.45	1.008

LOD calculation:

The calculation of limit of detection (LOD) was performed in a systematic manner. The standard deviation (σ) was calculated using the six-blank reading of MOF suspension in CH_3CN. The *K* value was obtained from the slop of the linear fit line of concentration verses fluorescence intensity plot (Figure S30). The above obtained parameters were used in the formula $3\sigma/K$ in order to get the LOD value.

The standard deviation σ for the blank reading of MOF suspension was calculated using the following formula as given below.

$$\sigma = \sqrt{\frac{\sum(x_i - \mu)^2}{N}}$$

Where, χ_i = Maxima of fluorescence intensities.

μ = The mean of all the maxima of fluorescence intensities.

N = The number of blank readings.

Table S2. Comparison table of different MOF probes for the sensing of Cu^{2+}.

S.I NO.	MOF	LOD	Detection time	Stern-Volmer constant (K_{sv})	Reference
1	PCN-222-Pd(II)	50 nM	30 min	N.A	2
2	$[Cd_2(PAM)_2(dpe)_2(H_2O)_2]\cdot 0.5(dpe)$	1 mM	N.A	N.A	3
3	Eu^{3+}@UiO-66-2COOH	1 nM	N.A	$5.35 \times 10^4\ M^{-1}$	4
4	MOF-525	67 nM	40 s	$4.5 \times 10^5\ M^{-1}$	5
5	Cd-MOF-74	78.7 µM	N.A	$1.81 \times 10^3\ M^{-1}$	6
6	$[Eu(pdc)_{1.5}(DMF)]\cdot(DMF)_{0.5}(H_2O)_{0.5}$	0.1 µM	N.A	$89.4\ M^{-1}$	7
7	$[NH_4]_2[ZnL]\cdot 6H_2O$	1 µM	N.A	N.A	8
8	$Zn(MeIM)_2\cdot(DMF)\cdot(H_2O)_3$	1 mM	N.A	N.A	9
9	$\{Mg(DHT)(DMF)_2\}n$	10 µM	N.A	$170.2\ M^{-1}$	10
10	$Eu(FBPT)(H_2O)(DMF)$	10 µM	N.A	N.A	11
11	$[Cd(H_2ttac)bpp]n$	0.63 mM	N.A	N.A	12

12	$[Eu_3(HCOO)_2(R\text{-}COO)_8]$	10 μM	N.A	$2.35 \times 10^3\ M^{-1}$	13
13	$\{[Mg_3(ndc)_{2.5}(HCO_2)_2(H_2O)][NH_2Me_2]\cdot 2H_2O\cdot DMF\}$	10 μM	N.A	$1.986 \times 10^3\ M^{-1}$	14
14	[Cd(2-aip)(bpy)]·2DMF	10 mM	10 s	N.A	15
15	$\{NH_2(CH_3)_2\cdot Cd_{2.5}(L)_2(H_2O)\cdot(H_2O)\}n$	0.1 mM	9 s	N.A	16
16	MIL-53-L	10 μM	N.A	$6.15 \times 10^3\ M^{-1}$	17
17	$[Eu(HL)(L)(H_2O)_2]\cdot 2H_2O$	10 μM	N.A	N.A	18
18	Zr-BPDC-$(SO_3H)_2$	0.22 μM	15s	$4.5 \times 10^5\ M^{-1}$	this work

References:

1. L. Zhou, W. Deng, Y. Wang, G. Xu, S. Yin and Q. Liu, *Inorg. Chem.*, 2016, **55**, 6271–6277.
2. Y. Chen and H. Jiang, *Chem. Mater.*, 2016, **28**, 6698–6704.
3. J. Ye, L. Zhao, R. F. Bogale, Y. Gao, X. Wang, X. Qian, S. Guo, J. Zhao and G. Ning, *Chem. Eur. J.*, 2015, **21**, 2029-2037.
4. X. Zhao, D. Liu, H. Huang and C. Zhong, *Microporous Mesoporous Mater.*, 2016, **224**, 149-154.
5. L. Li, S. Shen, R. Lin, Y. Bai and H. Liu, *Chem. Commun.* , 2017, **53**, 9986-9989.
6. T. Zheng, J. Zhao, Z. Fang, M. Li, C. Sun, X. Li, X. Wang and Z. Su, *Dalton Trans.*, 2017, **46**, 2456-2461.
7. B. Chen, L. Wang, Y. Xiao, F. R. Fronczek, M. Xue, Y. Cui and G. Qian, *Angew. Chem. Int. Ed.*, 2009, **48**, 500-503.
8. S. Liu, J. Li and F. Luo, *Inorg. Chem. Commun.*, 2010, **13**, 870-872.
9. S. Liu, Z. Xiang, Z. Hu, X. Zheng and D. Cao, *J. Mater. Chem.*, 2011, **21**, 6649-6653.
10. K. Jayaramulu, R. P. Narayanan, S. J. George and T. K. Maji, *Inorg. Chem.*, 2012, **51**, 10089–10091.
11. Z. Hao, X. Song, M. Zhu, X. Meng, S. Zhao, S. Su, W. Yang, S. Song and H. Zhang, *J. Mater. Chem. A*, 2013, **1**, 11043-11050.
12. L. Pang, G. Yang, J. Jin, M. Kang, A. Fu, Y. Wang and Q. Shi, *Cryst. Growth Des.*, 2014, **14**, 2954–2961.
13. B. Liu, W. Wu, L. Hou and Y. Wanga, *Chem. Commun.*, 2014, **50**, 8731-8734.
14. S. Bhattacharyya, A. Chakraborty, K. Jayaramulu, A. Hazra and T. K. Maji, *Chem. Commun.*, 2014, **50**, 13567-13570.
15. H. Wang, P. Liu, H. Chen, N. Xu, Z. Zhou and S. Zhuo, *RSC Adv.*, 2015, **5**, 65110-65113.

16. C. Qiao, X. Qu, Q. Yang, Q. Wei, G. Xie, S. Chen and D. Yang, *Green Chem.*, 2016, **18**, 951-956.
17. C. Liu and B. Yan, *Sensors and Actuators B*, 2016, **235**, 541–546.
18. Z. L, A. Liu, Y. Liu, J. Shen, C. Du and H. Hou, *Inorg. Chem. Commun.*, 2015, **56**, 137-140.